

First-principles simulations of glass-formers

Walter Kob* and Simona Ispas

Laboratoire Charles Coulomb,

UM-CNRS UMR 5221,

Université Montpellier,

Place Eugène Bataillon

F-34095 Montpellier, France

Abstract

In this article we review results of computer simulation of glasses carried out using first principles approaches, notably density functional theory. We start with a brief introduction to this method and compare the pros and cons of this approach with the ones of simulations with classical potentials. This is followed by a discussion of simulation results of various glass-forming systems that have been obtained via *ab initio* simulations and that demonstrate the usefulness of this approach to understand the properties of glasses on the microscopic level.

* walter.kob@umontpellier.fr

I. INTRODUCTION

In their early days, i.e. in 1940-1950, computer simulations were mainly used to address questions concerning the domain of statistical physics, such as the properties of hard sphere systems or the dynamics of simple crystals [1, 2]. A few decades later, i.e. when computers became more powerful and more accessible, researchers started to use simulations to study the properties of real materials. For this, people used an approach that today is referred to as “classical molecular dynamics”, i.e. the interactions between the particles that constitute the material are described by an effective potential with a form (e.g. Lennard-Jones) chosen in a rather *ad hoc* manner. The parameters of the potential (e.g. the depth and the position of the well in the Lennard-Jones potential) are chosen such that certain macroscopic properties of the simulated system (such as its density or the melting temperature of the crystal) match with the experimental data for the material. Once the interactions are known one solves numerically Newton’s equations of motion and hence obtains the trajectories of all the particles (for details see Chap. XX by A. Takada in the present volume [3], or Ref. [1]). From these trajectories one then can measure the physical properties of the system, such as the radial distribution function, the diffusion coefficient, or the mechanical properties such as the elastic constants.

Although simulation studies with effective potentials are very valuable to gain insight into the qualitative properties of liquids and solids, they usually do not allow to obtain a good *quantitative* description of a given specific material. The reason for this is that most material properties depend in a quite sensitive manner on the potential that describes the interactions between the particles that constitute the material. Since normally these interactions depend not only on the type of atoms considered, but also on the microscopic environment of the particles (e.g. the bond strength between an oxygen atom and a silicon atom will change if a hydrogen atom is approached to this pair), it is basically impossible to come up with a simple expression for the potential energy that is able to describe faithfully all these different environments. This problem is particularly pronounced for the case of glasses, since, in contrast to crystals, in these systems one has a multitude of very different local environments for each atom species. The only method that at present can address this problem in a systematic manner is the *ab initio* formalism. In this approach one does not rely on a fixed functional form for the interaction potential, but instead uses the electronic degrees

of freedom of each atom to compute the force that acts on each atom of the system. Once this force is known, one can use Newton's equations of motion to determine the trajectory of the particles and hence subsequently the properties of the system. Thus *a priori* the only input needed for these simulations are the species of the particles, a feature that has allowed *ab initio* simulations to become a highly interesting method to gain a detailed understanding of the properties of glass-forming liquids and glasses. The goal of this review is to give a brief introduction to the method, discuss its advantages but also its problems, and then to present some specific examples that show that this type of simulation is indeed very useful to improve our understanding of glasses on a microscopic scale. We will conclude with a brief outlook on what will be possible to do with *ab initio* simulations in the next few years.

II. AB INITIO SIMULATIONS

In the Introduction we mentioned that within the *ab initio* approach the forces on the atoms are obtained from their electronic degrees of freedom. The first step to do this is to start with the Schrödinger equation which describes the electronic degrees of freedom of the system and thus is given by

$$\mathcal{H}_e \Psi = E \Psi \quad , \quad (1)$$

where the (complex) many-electron wavefunction $\Psi(\{\mathbf{r}_i\}; \{\mathbf{R}_I\})$ depends on the positions of the n electrons, $\{\mathbf{r}_i\}$, as well as the positions of the N nuclei, $\{\mathbf{R}_I\}$ [4]. E is the energy of the electronic degrees of freedom, and the operator \mathcal{H}_e is given by

$$\mathcal{H}_e = - \sum_{i=1}^n \frac{1}{2} \nabla_i^2 + \sum_{\substack{i,j=1 \\ j < i}}^n \frac{1}{|\mathbf{r}_i - \mathbf{r}_j|} - \sum_{i=1}^n \sum_{I=1}^N \frac{Z_I}{|\mathbf{r}_i - \mathbf{R}_I|} \quad , \quad (2)$$

where Z_I is the charge of ion I . Note that this equation is written in atomic units, i.e. Planck's constant, the electronic charge and mass are set to unity, and the Laplacian ∇^2 is given by $\nabla^2 = \partial^2/\partial x^2 + \partial^2/\partial y^2 + \partial^2/\partial z^2$. We emphasize that in Eq. (1) only the electronic degrees of freedom are treated quantum mechanically whereas the ones of the nuclei are not. This approximation, often called "Born-Oppenheimer" or "adiabatic", is quite accurate since the mass of the electron is almost 2000 times smaller than the one of the lightest nucleus (i.e. the one of H). Hence the degrees of freedom of the electrons are basically decoupled from the

ones of the nuclei, i.e. the heavy nuclei move more slowly than the light electrons and the electrons adapt instantaneously to the changes of the nuclear positions. As a consequence it can be assumed that for the electronic structure calculation the nuclei are clamped at fixed positions and hence the electronic wavefunction Ψ depends on $\{\mathbf{R}_I\}$ only parametrically [5].

In order to reduce the computational complexity even further one considers only the ground state solution of Eq. (1), Ψ_0 , i.e. the state with the lowest energy. The interaction potential between the nuclei is then given by $\Phi(\{\mathbf{R}_J\}) = \langle \Psi_0 | \mathcal{H}_e | \Psi_0 \rangle + \sum_{I,J=1,J<I}^N \frac{Z_I Z_J}{|\mathbf{R}_I - \mathbf{R}_J|}$ and hence the force on particle I is given by $F_I = -\nabla_I \Phi(\{\mathbf{R}_J\})$ [5].

Finding the wavefunction Ψ_0 that is the solution of the Schrödinger equation (1) is a formidable task and there are two main approaches to do this: The first one is a wavefunction-based method, often known as the quantum chemistry approach, which starts from the Hartree-Fock method and, in a first order approximation, factorizes the many-body electronic wavefunction into one-particle wavefunctions. Subsequently one searches numerically for the ground state of this many-body wavefunction, a task that can be solved nowadays in a reasonable amount of computer time if the number of atoms is not too large, say, of order of some tens of atoms. Nevertheless one can note some recent works proposing new methods in this field with very promising results for systems containing some hundreds of atoms [6, 7].

The second method is the so-called “density functional theory” (DFT), a formalism that exploits certain ground state properties of a many-electrons system in an external field, thus in our case the Coulomb field of the nuclei. Following up ideas proposed by Thomas and Fermi in the 1930’s, the current DFT formalism has been rigorously established by Hohenberg, Kohn, and Sham [8–10] in the early 60’s. DFT gets rid of the many-body wavefunction, that depends on $3 \times n$ electronic spatial coordinates, and replaces it by the more simple electronic density $\rho(\mathbf{r})$ that depends only on three spatial coordinates:

$$\rho(\mathbf{r}) = \int \dots \int d\mathbf{r}_2 \dots d\mathbf{r}_n \Psi_0^*(\mathbf{r}, \mathbf{r}_2, \dots, \mathbf{r}_n) \Psi_0(\mathbf{r}, \mathbf{r}_2, \dots, \mathbf{r}_n). \quad (3)$$

Kohn and Sham [9] showed that this density can be written as a sum of the density of non-interacting particles, $\rho(\mathbf{r}) = \sum_i^n |\phi_i(\mathbf{r})|^2$, where ϕ_i are the fictitious one-particle Kohn-Sham (KS) orbitals, and thus the ground state density $\rho_0(r)$ is given by the sum of the ground states of these particles. Hence the total energy of the system can be expressed as

$$E_{\text{KS}}[\rho] = E_{\text{kin}}[\rho] + \int d\mathbf{r} \rho(\mathbf{r}) \left[\frac{1}{2} \int d\mathbf{r}' \frac{\rho(\mathbf{r}')}{|\mathbf{r} - \mathbf{r}'|} - \sum_I \frac{Z_I}{|\mathbf{r}_i - \mathbf{R}_I|} \right] + E_{\text{xc}}[\rho]. \quad (4)$$

Here $E_{\text{kin}}[\rho]$ is the kinetic energy of a system of n non-interacting electrons having the density ρ : $E_{\text{kin}} = -\frac{1}{2} \sum_{i=1}^n \int d\mathbf{r} \phi_i^*(\mathbf{r}) \nabla^2 \phi_i(\mathbf{r})$. The second term represents the Coulomb interactions between electron-electron and electron-nuclei. The third term is the so-called exchange-correlation (XC) energy and it accounts for all quantum many-body effects due to the Pauli exclusion principle which introduces correlations between the electrons. Since this term cannot be evaluated exactly, approximations have to be made. Even if it is found that $E_{\text{xc}}[\rho]$ is usually substantially smaller than those of the two other terms, the choice of its approximation may become crucial for chemically complex systems [11, 12]. The simplest one, proposed originally by Kohn and Sham [9], relies on the assumption that at each point the exchange-correlation energy density corresponds to the one of a homogeneous gas of electrons. This approximation is called the ‘‘Local Density Approximation’’ (LDA) and is given by:

$$E_{\text{xc}}^{\text{LDA}}[\rho(\mathbf{r})] = \int d\mathbf{r} \rho(\mathbf{r}) \varepsilon_{\text{xc}}^{\text{LDA}}[\rho(\mathbf{r})]. \quad (5)$$

We note that even for such a simple model system the expression of the correlation energy has to be calculated numerically using Monte Carlo methods. Some more advanced approximations, the so-called ‘‘Generalized Gradient Approximation’’ or GGA, are based on more complex operators making use of the density gradient of m th order

$$E_{\text{xc}}^{\text{GGA}}[\rho(\mathbf{r})] = \int d\mathbf{r} \rho(\mathbf{r}) \varepsilon_{\text{xc}}^{\text{GGA}}[\rho(\mathbf{r}); \nabla^m \rho(\mathbf{r})]. \quad (6)$$

However, it is not always the case that these higher approximations give more reliable results and hence it is *a priori* not always clear which exchange functional should be used [11, 12]. Despite this problem one can say that the Kohn-Sham approach and reasonable (simple) approximations for the exchange correlation term have opened the door to the calculations of the electronic structure for many-atom systems in order to study real materials.

Although expressing the full quantum mechanical problem in the language of DFT leads to a significant reduction of the computational effort for calculating the forces on the nuclei, it is found that in practice this task is still extremely demanding once one has more than a few tens of atoms. Therefore one usually makes the further approximation that all the core

electrons of an atom are lumped together and their effect is replaced by an effective potential, the so-called “pseudo-potential”, for the remaining valence electrons which are described by a pseudo-wavefunction [4, 5]. The physical motivation for this approximation is that the chemical bonds between two atoms are usually related to the outer valence electrons and depend only weakly on the inner core electrons.

So far we have discussed how DFT allows to obtain the forces exerted on the nuclei due to their surrounding electrons. These forces can now be used to solve the equations of motion for the nuclei

$$M_I \ddot{\mathbf{R}}_I = -\nabla_I E_{KS} [\{\phi_i\}, \mathbf{R}] \quad , \quad (7)$$

where the energy $E_{KS} [\{\phi_i\}, \mathbf{R}]$ can be calculated from the KS orbitals within the Kohn-Sham scheme of the DFT. In the above equations the nuclei are considered as classical particles and Eqs. (7) are solved using the same methods as in classical MD (see Chap. XX by Takada [3] or [1, 2] for details on how classical simulations are done). Due to the resulting motion of the ions, the electronic structure changes and hence one has in principle to recalculate the total energy of the electronic ground state, a procedure that remains, despite the DFT approach, computationally very costly. One possibility to avoid this problem was proposed in a seminal paper by Car and Parrinello in 1985 [13]. The idea of that approach, today called Car-Parrinello Molecular Dynamics (CPMD), is to introduce a fictive dynamics to the electronic degrees of freedom and thus recast the quantum mechanical problem into a classical problem with the electronic wave-functions as new effective degrees of freedom. Although the CPMD approach allows to obtain the correct equilibrium properties of a system, the introduction of the fictive dynamics for the electronic degrees of freedom makes that the motion of the system in configuration space is not completely realistic [5]. Despite this shortcoming, CPMD simulations have been and still are widely used to study complex systems by means of computer simulations (see for example Refs. [14–16]). (On <http://www.psi-k.org/codes.shtml> one can find the necessary software to do such simulations.) The mentioned problem can, however, be avoided within the so-called Born-Oppenheimer molecular dynamics (BOMD) in which one solves at each time step the electronic problem. This approach allows thus to give a correct dynamics but this at the cost of a increased computational load. Only in the last few years the numerical algorithms have been improved to such an extent that today it is possible to simulate within BOMD several hundreds particles [17–20].

	Classical MD	<i>Ab Initio</i> MD
Number of atoms	1 000 - 500 000	100 - 500
Box size	$\sim 100 \text{ \AA}$	$\sim 15\text{-}20\text{\AA}$
Trajectory length	$\sim 1 \text{ ns} - 10 \text{ }\mu\text{s}$	$\sim 20 - 100 \text{ ps}$
Transferability	sometimes	yes

TABLE I. Comparison of various features of large scale computer simulations carried out with classical and *ab initio* methods.

The brief description of the *ab initio* simulations that we have given so far should make it clear that in practice the computer code to carry out such simulations must be extremely optimized in order to keep the necessary computer time for the simulations within a reasonable limit. Therefore it is not really advisable that a researcher writes his/her proper code, in contrast to the situation of simulation with effective potentials. Instead people use one of the packages that have been developed over the years and that are very sophisticated and highly optimized. Various groups use different approaches to maintain and develop these packages, the most popular ones being Car-Parrinello (CPMD), VASP, Quantum Espresso, CP2K, Siesta, CASTEP, etc... (see on <http://www.psi-k.org/codes.shtml> for a more extended list). Each of these packages has advantages and disadvantages regarding the scaling of computational effort with system size, accuracy, ensembles that can be simulated (microcanonical, canonical, constant pressure, ...), quantities that can be calculated, etc. and therefore it is not really possible to say which one is the best.

In order to give an idea on what at present can be done with such *ab initio* simulations we present in Table I a brief comparison between *ab initio* simulations and classical simulations. Since the computational load for the *ab initio* simulations does depend in a non-negligible manner on the system considered (due to the different electronic structure for the atoms), we consider the example of a glass containing oxide. We note that the above numbers are valid for a certain amount of computer time and of course one has the choice to trade the number of atoms versus the time span covered in the simulation. For a classical system the relevant number is basically the product of the two quantities, i.e. doubling the system size will increase the necessary computer time by a factor close to two. For *ab initio* simulation the situation is not that favorable, since doubling of the system size usually leads to an increase of

the computational load by a factor of 2^α , with α on the order of 3. As a consequence *ab initio* simulations do not only have smaller system sizes but also the accessible time scale is smaller than the ones in classical simulations. Therefore the quench rates that are used to cool a system from its liquid state to its glass state are usually on the order of $10^{13} - 10^{15}$ K/s, rates that are thus significantly larger than the ones used in classical simulations ($10^{10} - 10^{14}$ K/s) and of course much larger than the experimental rates ($10^{-2} - 10^6$ K/s). However, despite these huge differences in cooling rates, the resulting glasses are surprisingly similar, since many of their properties depend only in a logarithmic way on these rates. Therefore it does make sense to use *ab initio* simulations to investigate the properties of glasses on the microscopic scale.

III. STRUCTURAL PROPERTIES

The goal of this section is to present some examples that demonstrate how *ab initio* simulations can help to gain a better understanding of the local structure of complex glasses. Since the literature on this topic is already quite substantial, it is not possible to discuss all the results that have been obtained so far, but we will mention at least some of the relevant ones.

The very first *ab initio* MD simulations for a glass-former were carried out by Sarnthein *et al.* in 1995 who considered the archetypical glass-former silica [21, 22]. Using the Car-Parrinello approach, they generated a glass model by equilibrating for 10 ps a liquid sample with 72 atoms (!) at 3500 K and subsequently quenching it to $T = 0$ K. Despite the smallness of the system and the high quench rate (10^{15} K/s!), the resulting glass structure was surprisingly similar to the one of the real material in that, e.g., the neutron structure factor was compatible with the one obtained from scattering experiments. As expected, the network in the glass was built from SiO_4 corner-sharing tetrahedra. These authors calculated also the electronic density of states and found it to match well with the one obtained from x-ray photoelectron spectroscopy experiments, although the predicted band gap of 5.6 eV underestimated the experimental value of about 9 eV, a flaw that often occurs in DFT calculations [23]. In these papers also the vibrational properties of the glass were determined and below we will come back to these results.

This pioneering paper was followed up by further studies in which more complex glass-

formers were studied, such as alkali silicate glasses, calcium-alumino-silicates [24–33], and other glass formers [34–37]. These investigations allowed to obtain detailed insight into the local arrangement of the atoms, how network modifiers like Na or Ca modify these arrangements, to connect the local structure in real space with the structural features as determined in neutron or x-ray scattering experiments, as well the vibrational features discussed in the next section.

As an example on what type of structural information present day *ab initio* simulations can provide we will now briefly discuss some results obtained for a sodium borosilicate of composition 30% Na₂O-10% B₂O₃-60% SiO₂(NBS), a glass-former that is the basis of many glasses found in our daily life. In addition this system is interesting since the boron atoms can form bonds with three or four oxygen neighbors, which makes that the structure of this system is rather complex [18, 19]. One of the most important quantities to characterize the structure are the partial radial distribution functions $g_{\alpha\beta}(r)$ which are directly proportional to the probability that two atoms of type α and β are found at a distance r from each other. Thus this function is defined as [38, 39]

$$g_{\alpha\beta}(r) = \frac{V}{4\pi r^2 N_\alpha (N_\beta - \delta_{\alpha\beta})} \sum_{i=1}^{N_\alpha} \sum_{j=1}^{N_\beta} \langle \delta(r - |\vec{r}_i - \vec{r}_j|) \rangle \quad , \quad (8)$$

where $\langle . \rangle$ represents the thermal average, V is the volume of the simulation box, N_α is the number of particles of species α , and $\delta_{\alpha\beta}$ is the Kronecker delta.

In the upper panel of Fig. 1 we show the radial distribution function for the boron-oxygen pair, focusing on the first nearest neighbor peak. We see that this peak (bold solid black curve) is relatively large and slightly asymmetric. By considering the two principal environments of a boron atom (three and four fold coordinated boron atoms, ^[3]B and ^[4]B, respectively), we can decompose this peak into two contributions (thin solid and dashed lines, respectively). This allows us to understand that the broadening of the total peak is a consequence of the presence of these two populations, with the bond distance ^[3]B–O giving rise to the smaller distances and the ^[4]B–O bonds to the large distances. The distributions for these two distances can be further decomposed by considering the nature of the second nearest neighbor of the central boron atoms, i.e. whether the nearest oxygen is connected to a Si or B atom, or whether it is a non-bridging oxygen. We see that for the case of the ^[3]B atoms, the nature of this second nearest neighbor species influences the B–O distance

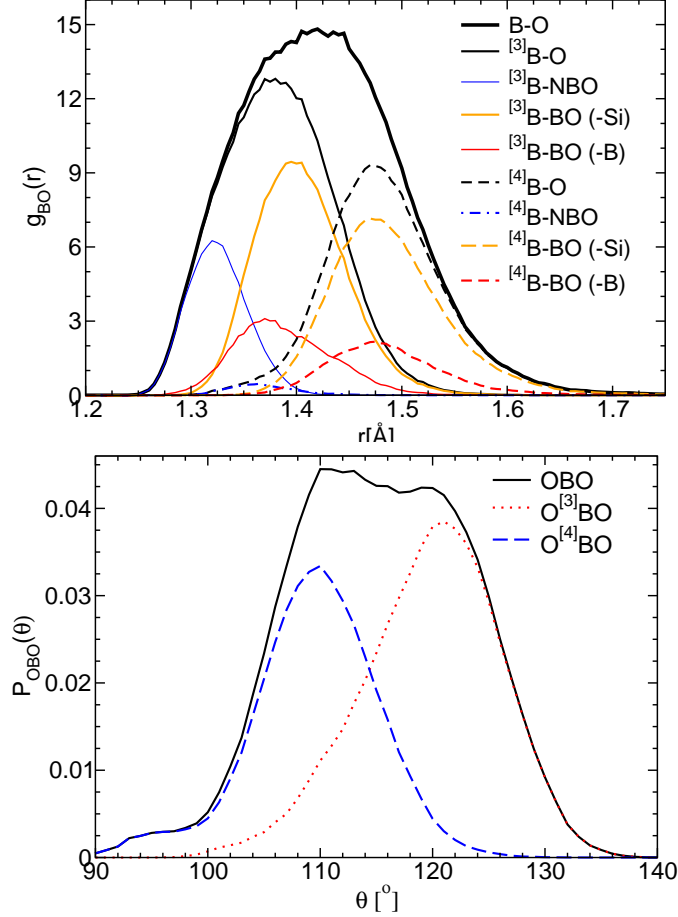


FIG. 1. Top: First peak of the partial radial distribution function $g_{BO}(r)$ of the NBS glass. The total peak has been decomposed into the various contributions from the different environments around a boron atom. Bottom: Distribution of the angle formed by two oxygen atoms that are connected to the same boron atom. This distribution is decomposed into contributions in which the central boron atoms is of type $^{[3]}B$ or type $^{[4]}B$ (dashed and dotted line, respectively). From Ref. [19].

since the position of the corresponding peak depends on the species, whereas this is not the case for the length of the $^{[4]}B-O$ bonds.

In the lower panel of Fig. 1 we show the distribution function for the central angle formed by an $O-B-O$ triplet (bold black line). One sees that this distribution has two peaks and again they can be traced back to the presence of $^{[3]}B$ and $^{[4]}B$ structural units (dashed and dotted lines, respectively).

At this point we emphasize that all these structural details can only be obtained be-

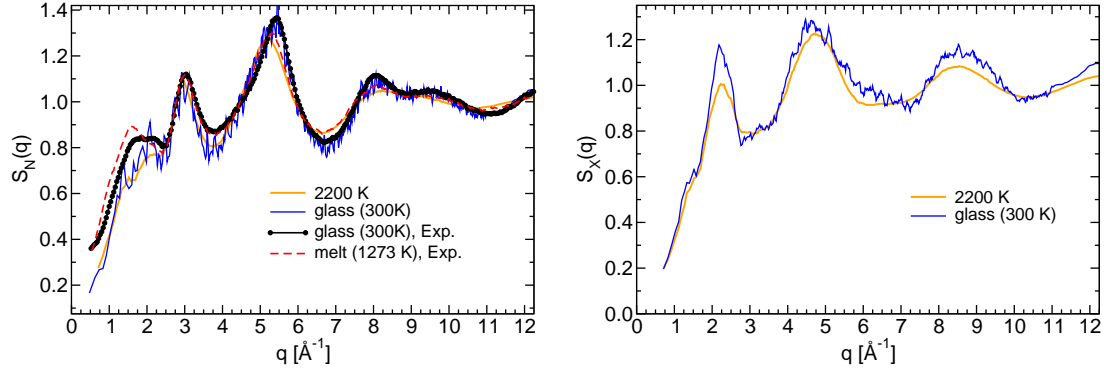


FIG. 2. Neutron and x-ray structural factors (left and right panel, respectively) for a borosilicate system in the liquid and glass state. Adapted from Ref. [18].

cause the structure obtained from the *ab initio* simulations is, at least locally, very accurate. Although one can of course make the same type of analysis for structures that have been obtained from a simulation with an effective force field, it is quite unlikely that an effective potential is able to reproduce the correct physics (charge transfer between the atoms, ...) involved in the formation of these local structures corresponding to different coordination states. In contrast to this, one expects quantities like the positions of the peak and the sub-peaks, their heights or broadening etc. will be correctly reproduced by an *ab initio* simulations. Thus for this type of details and especially for glasses with complex compositions the use of *ab initio* simulations is mandatory. We also mention that for chalcogenide glasses, there are at present no force-fields available that are able to describe correctly the homopolar bonds.

The detailed structural information shown in Fig. 1 is very valuable to obtain a better understanding of the local structure of the glass. It is, however, also important to connect the results from the simulation with experimental data. Although experiments on atomic systems do not allow to access directly the radial distribution functions, it is possible to measure the static structure factor which is directly related to the weighted sum of $S_{\alpha\beta}(q)$, the space Fourier transform of $g_{\alpha\beta}(r)$ [39]. For the case of neutron scattering the connection is given by

$$S_N(q) = \frac{N}{\sum_{\alpha} N_{\alpha} b_{\alpha}^2} \sum_{\alpha, \beta} b_{\alpha} b_{\beta} S_{\alpha\beta}(q) \quad . \quad (9)$$

Here b_{α} are the neutron scattering length [40] and the partial static structure factors are

given by

$$S_{\alpha\beta}(q) = \frac{f_{\alpha\beta}}{N} \sum_{j=1}^{N_\alpha} \sum_{k=1}^{N_\beta} \langle \exp(i\mathbf{q} \cdot (\mathbf{r}_j - \mathbf{r}_k)) \rangle, \quad (10)$$

where $f_{\alpha\beta} = 1$ for $\alpha = \beta$ and $f_{\alpha\beta} = 1/2$ otherwise and N is the total number of atoms. For the case of x-ray scattering the relation is

$$S_X(q) = \frac{N}{\sum_\alpha N_\alpha f_\alpha^2(q/4\pi)} \sum_{\alpha,\beta} f_\alpha(q/4\pi) f_\beta(q/4\pi) S_{\alpha\beta}(q), \quad (11)$$

where $f_\alpha(s)$ is the scattering-factor function (also called form factor) and its value can be found in Ref. [41]. For the case of NBS the q -dependence of $S_N(q)$ and $S_X(q)$ is shown in Fig. 2 and we recognize that the two functions are rather different despite the fact that they have been obtained from exactly the same glass sample. The reason for this is that these structure factors are a *weighted* sum of the partial structure factors, each of which has a multitude of positive and negative peaks. Since the weight depends on whether one considers neutron or x-ray scattering, the resulting sum might show a peak for, say, $S_N(q)$ whereas this feature is basically absent in $S_X(q)$. Since in systems with k species one has $k(k+1)/2$ partial structure factors, the interpretation of the various peaks in experimental data can become rather difficult. It is in such cases that the structure factor as obtained from computer simulations can help to get the correct interpretation of the various peaks, but this only under the condition that the positions and height of the different peaks in the partial structure factors are reproduced reliably, and this is usually only the case with *ab initio* simulations.

So far we have considered simulations of bulk systems. Another important situation in which simulations can help to gain a better understanding of the structure are surfaces, since in this case experimental scattering techniques are much less powerful to obtain microscopic information since one has to use grazing ray geometries. Although in principle it is no problem to use simulations to investigate surfaces, in such studies one is faced with the issue that basically all effective potentials have been developed for *bulk* systems and there is no guarantee that they will be reliable for surfaces in which the local structures can be very different from the ones in the bulk (e.g. for the case of pure silica one finds at the surface an appreciable concentration of two membered closed rings, a structure that is completely absent in the bulk). Hence for such simulations it is strongly preferable to use *ab*

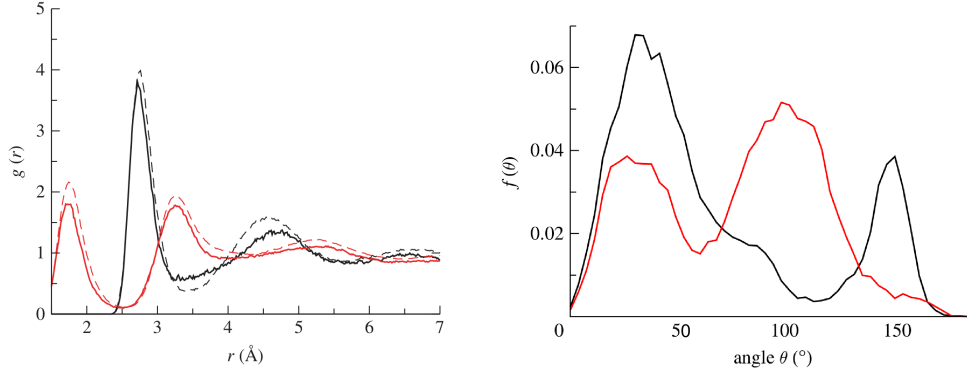


FIG. 3. Left panel: Water-water radial distribution functions for surface water (SW) and bulk water (BW): black continuous line, O-O (SW); red continuous line, O-H (SW); black dashed line, O-O (BW); red dashed line, O-H (BW). Right panel: Distribution of the angle θ between the water dipole (bisecting the HOH angle) and the surface normal, for SW and BW molecules: black solid line, SW; red solid line, BW. Figures extracted from Ref. [42].

initio simulations since they allow without adjustments of any parameter to deal with such heterogeneous geometries. As an example for such a simulation we show in the left panel of Fig. 3 the partial radial distribution functions for H–O and O–O of water that is close to a surface of amorphous silica (full lines) [42]. For the sake of comparison the graph also includes the corresponding distributions for bulk water (dashed lines). The curves clearly show that there is no significant difference between bulk and surface water with respect to the position of the various peaks. However, for the water close to the surface, the height of the peaks is lower than the one for the bulk system thus showing that close to the surface the fluid is less structured than in the bulk. Since these modifications are not very pronounced, it is important to study such effects using interaction potentials that are very reliable, and thus one has to use *ab initio* simulations. In the right panel of Fig. 3 we show the angle between water dipole (i.e. the bisector of the HOH angle) and the surface normal for the water in the bulk state as well for water close to the surface and we recognize that these distributions are very different, thus showing that the presence of the surface leads to a strong change of the local geometry. To conclude this section on the structure of glasses we mention that *ab initio* simulations are not only very useful, read mandatory, if the system has many different components, but also if the glass contains water [28], a molecule that due to its reactivity is very difficult to simulate by means of effective potentials.

IV. VIBRATIONAL PROPERTIES

The structural features of glasses are important for their mechanical properties as well as for some transport properties (e.g. in ion conducting glasses). On the other hand there are many quantities that depend directly or indirectly on the vibrational properties of the system, such as the specific heat, the conduction of heat, the transparency of the material, etc. Therefore it is of great interest to study also these vibrational properties in detail.

We remind the reader that the vibrational density of states (vDOS) $g(\omega)$, is the normalized distribution function of the eigenfrequencies ω_p of the dynamical matrix of the system (which in turn is directly related to the second derivative of the potential with respect to the coordinates \vec{r}_i and \vec{r}_j , i.e. $\partial^2 U_{pot}/\partial\vec{r}_i\partial\vec{r}_j$), thus

$$g(\omega) = \frac{1}{3N - 3} \sum_{p=4}^{3N} \delta(\omega - \omega_p) . \quad (12)$$

Here one divides by $3N - 3$, the number of eigenmodes with non-zero frequency. Associated with each eigenfrequency ω_p of the dynamical matrix is an eigenvector \mathbf{e}_p that gives detailed information regarding the particles that oscillate with the frequency ω_p . Such studies have allowed to gain insight into the nature of the vibrational modes of various materials such as silica and germania glasses [34, 43–47] as well as more complex systems [19, 29, 32, 48–50].

Note that the true vDOS given by Eq. (12) is not directly accessible in experiments, in which only an effective vDOS: $G(\omega) = C(\omega)g(\omega)$ can be measured. The correction function $C(\omega)$ describes how the modes with frequency ω are coupled to the probing beam of the experiment (photons, neutrons,...) [51]. For the case of inelastic neutron scattering experiments, this function can be calculated, within approximations, from the eigenvectors \mathbf{e}_p of the dynamical matrix [52].

In practice there are two possibilities to calculate the vibrational properties of a system. The first one is to determine the local potential minimum of the glass structure (i.e. to quench the sample to $T = 0$ K) and then to calculate directly the dynamical matrix, e.g. by using a finite difference scheme for the forces. By diagonalizing this matrix one can then obtain its eigenfrequencies and eigenvectors and hence $g(\omega)$. The second method consists in running a simulation in which one solves Newton's equations of motion, and one measures the time auto-correlation function of the velocity of a particle. It can be shown that the time Fourier transform of this velocity auto-correlation is directly proportional to the vibrational

density of states at low temperatures, i.e. in a regime in which the harmonic approximation is valid [51]. For higher temperature, a density of state computed using this approach can present modifications with respect to the one at low temperatures, which can originate from anharmonic effects. We note that the approach with the auto-correlation function is from the computational point of view inexpensive, but it has the drawback that it does not give any information on the eigenvectors, i.e. the nature of the motion of the atoms.

In the previous section we have argued that often *ab initio* simulations are mandatory to get a good qualitative description of the local atomistic structure. Experience shows that this is even more the case if one wants to study the vibrational properties of a glass. Roughly speaking the reason for this is that the structure is related to a balance of the forces between the particles, i.e. the *first* derivative of the potential, since these forces have basically to compensate in order to get a mechanically stable structure. In contrast to this the vibrational properties are related to the curvature of the potential, i.e. its *second* derivatives. As a consequence it is in practice quite hard to find effective potentials that are able to reproduce the experimental vibrational density of states and in fact this is the case even for systems as simple as pure silica [53].

As an example for this we show in Fig. 4 the neutron effective vDOS for silica as it has been obtained by means of a simulation with the effective potential proposed by van Beest, Kramers, and van Santen [54] which is able to give a surprisingly good description of the structural properties of real silica [55]. Also included in the figure is the *ab initio* data from a small sample of SiO₂ (78 atoms) [45]. We see that the two predictions are quite similar regarding the vDOS at high frequencies, i.e. the modes concerning intra-tetrahedral excitations [43]. However, for frequencies between 200 and 600 cm⁻¹ the two calculated spectra differ significantly in that the *ab initio* data shows a marked peak at around 400 cm⁻¹ whereas the BKS data is basically flat. A comparison with the experimental data (symbols) shows that there is indeed a peak in that frequency range, i.e. that the prediction of the *ab initio* simulation is correct, and this despite the smallness of the sample. Thus we can conclude that although from the point of view of structure the BKS potential is quite reliable, it fails to reproduce some of the vibrational features found in real silica. More details on this point can be found in Ref. [45].

A further technique that is used in experiments to get insight into the vibrational properties of glasses are dielectric measurements (see Chap. XX in the present volume by G. Hen-

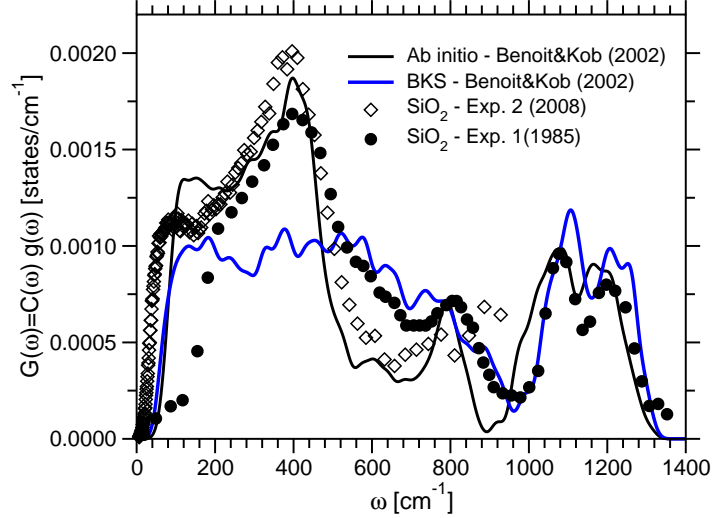


FIG. 4. Effective neutron densities of states (vDOS) for a-SiO₂ as obtained from an *ab initio* simulation (solid black line) and a simulation with an effective force field (BKS, solid blue line) [45]. Also included is data from two type of neutron scattering experiments (symbols) [56, 57].

person [58]). Since this quantity is directly related to the local polarizability of the material, it is mandatory that the simulation does give a good description of this polarizability and for the *ab initio* approach this is indeed the case [59] thus allowing to access directly the high-frequency and static dielectric constant. The previous, ϵ_∞ , can be estimated as one third of the trace of the purely electronic dielectric tensor $(\epsilon_\infty)_{ij} = \delta_{ij} + \frac{4\pi}{V} \frac{\partial^2 E_{tot}}{\partial \mathcal{E}_i \partial \mathcal{E}_j}$ (also called relative permittivity), a tensor that describes the reaction of the electrons to the presence of an external electric field under the condition that the ions are kept at fixed positions. In practice it is found that for glasses this tensor is basically isotropic and diagonal. The static dielectric constant ϵ_0 reflects the ionic displacement contributions to the dielectric constant and it can be expressed as [60]:

$$\epsilon_0 = \epsilon_\infty + \frac{4\pi}{3V} \sum_p \sum_j \frac{|\mathcal{F}_j^p|^2}{\omega_p} , \quad (13)$$

where p runs over all the eigenmodes, $j \in \{x, y, z\}$, and \mathcal{F}_j^p is the so-called oscillator strength which is defined as

$$\mathcal{F}_j^p = \sum_{I,k} \frac{\mathbf{e}_{I,k}(\omega_p)}{\sqrt{m_I}} Z_{I,jk} . \quad (14)$$

Here $\mathbf{e}_{I,k}(\omega_p)$ is that part of the eigenvector $\mathbf{e}(\omega_p)$ that contains the 3 components related

to the displacement of particle I , and the quantity $Z_{I,jk}$ is the Born effective charge tensor $Z_{I,jk}$ which is given by

$$Z_{I,ij} = \frac{\partial F_i^I}{e \partial \mathcal{E}_j} \quad I = 1, 2, \dots, N, \quad i, j \in \{x, y, z\}, \quad (15)$$

where e is the elementary charge, i.e. $Z_{I,ij}$ is an effective charge that connects the strength of an external electric field \mathcal{E} to the force \mathbf{F}^I acting on particle I .

From these quantities one can now obtain immediately the real and imaginary parts of the dielectric function $\epsilon(\omega) = \epsilon_1(\omega) + i\epsilon_2(\omega)$ [60, 61]:

$$\epsilon_1(\omega) = \epsilon_\infty - \frac{4\pi}{3V} \sum_p \sum_j \frac{|\mathcal{F}_j^p|^2}{\omega^2 - \omega_p^2} \quad (16)$$

$$\epsilon_2(\omega) = \frac{4\pi^2}{3V} \sum_p \sum_j \frac{|\mathcal{F}_j^p|^2}{2\omega_p^2} \delta(\omega - \omega_n). \quad (17)$$

Closely related to $\epsilon(\omega)$ is the absorption spectra $\alpha(\omega)$ which is given by [62]

$$\alpha(\omega) = 4\pi\omega n''(\omega) \quad , \quad \text{with } n''(\omega) = \sqrt{\frac{\sqrt{\epsilon_1^2 + \epsilon_2^2} - \epsilon_1}{2}} \quad . \quad (18)$$

Since all these functions can be measured directly in experiments they allow on one side to test the predictive power of the simulations and on the other hand help to interpret the various features found in the experimental spectra. Examples for this are presented in Fig. 5 where the left panel shows a comparison between the infra-red spectrum of amorphous silica, Ref. [63], and the spectrum obtained from an *ab initio* simulation [46]. One clearly sees that the theoretical calculation is able to predict reliably the position of the various peaks, although their width does not match very well the experimental data [46]. In the right panel of the figure we show the corresponding theoretical spectra for a more complex glass, namely NBS, and compare it with experimental data. From the upper panel we see that this glass shows below 300 cm^{-1} a broad band. Since in this frequency range the vDOS is strongly dominated by the motion of Na atoms [19], we can conclude that this band is related to that atomic species, which explains why the spectra of the glass-formers that do not contain alkali atoms do not show such a low frequency band. In addition the spectra for NBS shows a narrow band slightly above 400 cm^{-1} . This feature is also present in the spectrum of pure silica and is known to originate from the bending and rocking motion

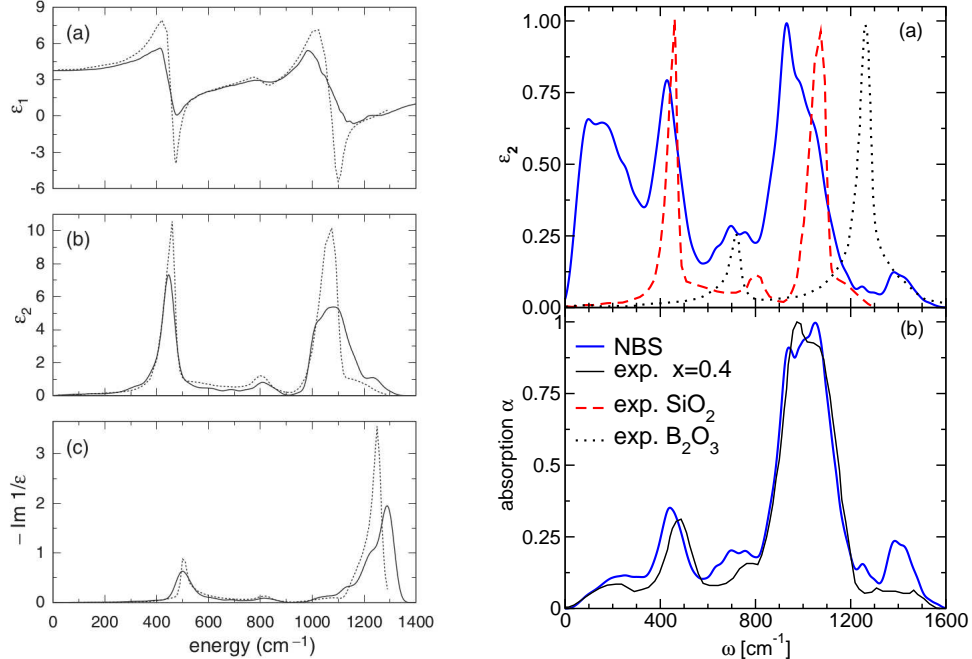


FIG. 5. Left panel: Infrared spectra for amorphous SiO_2 as obtained from *ab initio* simulations (solid lines) and from experiments (dotted lines) [46]. Right panel: Infrared spectra for a sodium borosilicate glass as obtained from *ab initio* calculations [19] and compared to experimental data for pure SiO_2 and B_2O_3 glasses, as well as for a sodium borosilicate glass with a similar composition (for more details see Ref. [19]).

of oxygen atoms [44, 64]. Therefore it is likely that for the NBS glass the origin of the corresponding peak is the same, although we see that for this glass the peak is somewhat broader and shifted to lower frequencies. These observations can be rationalized by the fact that the structure of the NBS glass is more disordered than the one of pure SiO_2 .

At high frequencies we can distinguish two bands. The first one ranges from 850 to 1200 cm^{-1} , and it can be assigned to oxygen stretching modes of Si-O bonds [65, 66]. The fact that for NBS this band is at lower frequencies than the corresponding band for silica (sharp peak at around 1070 cm^{-1}) is consistent with earlier results which showed that the presence of non-bridging oxygen atoms leads to a shift of the band to lower frequencies [48]. The second high-frequency band, extending between 1200 and 1600 cm^{-1} , is due to the motions of oxygen atoms belonging to $^{[3]}\text{B}$, i.e. boron atoms that are connected to exactly three oxygen atoms. This is supported by a comparison with the experimental data for B_2O_3 , which has only $^{[3]}\text{B}$ units, and which shows that the latter has a very pronounced

peak in this frequency range.

Finally we show in the lower right panel of Fig. 5 the absorption spectrum of NBS as obtained from *ab initio* simulations as well as the corresponding experimental data for a very similar glass composition [62]. We see that the theoretical curve matches very well the experimental data. The main deviation is found at high frequency in that there the simulation data shows a marked peak which is absent in the experimental spectrum. The reason for this difference can be traced back to the fact that the simulation sample has a too high concentration of ^{10}B units and that these units give rise to a marked peak in that frequency range [19]. However, despite this minor flaw we can conclude that the *ab initio* simulation is able to make a surprisingly good prediction of this quantity.

Finally we mention that DFT based methods have also been proposed in order to compute Raman and hyper-Raman spectra for periodic solids [67, 68]. These approaches have been used to calculate the corresponding spectra for the main oxide network-formers, i.e. SiO_2 , B_2O_3 or GeO_2 , and it has been found that they are able to give a good description of the experimental data [34, 36, 46, 69–71].

V. NMR SPECTRA

We conclude with a brief discussion on the calculation of nuclear magnetic resonance (NMR) spectra within the framework of DFT. Solid state NMR is a technique that allows to obtain detailed insight into the local structure of materials (see Chap. XX by J. F. Stebbins in the present volume [72]). Thus this approach is particularly fruitful if the system lacks crystalline symmetry, this in contrast to standard scattering experiments. However, one problem that one faces with NMR experiments on disordered structures is that sometimes the various peaks in the measured signal superpose each other and thus it is not straightforward to come up with a real space interpretation of the obtained spectrum. It is therefore most useful if a theoretical calculation can give some guidance for such an interpretation. However, coming up with a practical computational method that allows to do such calculations for bulk system is not that easy and in fact schemes to carried out this kind of calculation were proposed only 15 years ago [73, 74]. In the glass community, the so-called GIPAW approach proposed by Pickard and Mauri [73] is certainly the most used one, and implemented in many *ab initio* packages. However, the theory on how this is done is somewhat involved and

therefore we do not present it here but instead refer to a recent review on that topic, see Ref. [75].

In the left panel of Fig. 6 we compare for different glasses experimental NMR data with theoretical prediction. We see that the agreement is surprisingly good in that the location of the peaks of the theoretical spectra reproduces well the one of the experiment. Deviations are sometimes seen in the relative intensity of the peaks (see, e.g. the case of the lithium-silicate glass). It is likely that these discrepancies are only partly related to the inaccuracy of the theoretical calculation of the spectrum, but instead also to the too large quench rates used to produce these samples as well as to their rather modest size. E.g. in the NBS system discussed above the concentration of $^{[3]}\text{B}$ decreases with the cooling rate whereas the one of $^{[4]}\text{B}$ increases [19], which can be expected to affect the intensity of the various peaks. However, with a bit of effort it is possible to handle this problem by probing how the concentration of the various local structures depend on the cooling rate (or on the temperature of the liquid) and then to extrapolate these concentrations to experimental cooling rates [19].

Although NMR experiments are able to provide information regarding the nature of the local structure ($Q^{(n)}$ -species, connectivity of the atoms,...) it is very difficult to extract direct information on the geometry of the local structures, such as bond angles. This information can of course be obtained directly from the *ab initio* simulations and one finds that the NMR signal is indeed sensitive to these angles. This is demonstrated in the right panel of Fig. 6 where we show for various glasses how the chemical shift for an Si atom depends on the angle formed by Si-O-T, where the O is a first nearest neighbor oxygen atom of the Si atom and T the second Si atom that is bonded to that O atom. The data clearly shows that: 1) there is a linear relation between this angle and the chemical shift; 2) that this relation is basically independent of the composition of the glass; and 3) that the slope depends on the $Q^{(n)}$ -species of the second Si atom. From these results one can thus conclude that the NMR spectra do *a priori* contain information not only on the nature of the local structure, but also on their geometry.

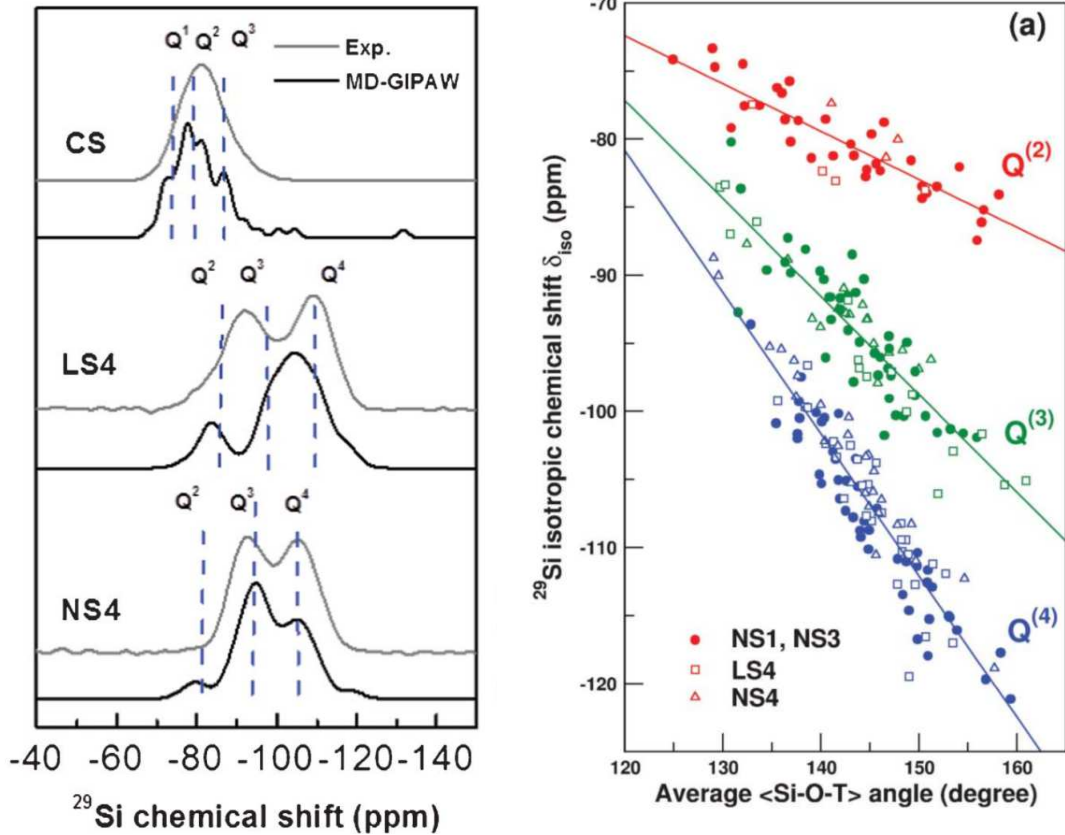


FIG. 6. Left panel: Theoretical and experimental ^{29}Si magic angle spinning NMR spectra of a sodium tetrasilicate glass (molar composition $20\text{Na}_2\text{O}-80\text{SiO}_2$, labelled NS4), a lithium tetrasilicate glass (molar composition $20\text{Li}_2\text{O}-80\text{SiO}_2$, labelled LS4), and a calcium silicate glass ($50\text{CaO}-50\text{SiO}_2$, labelled CS). This panel, extracted from Ref. [76], compiles data reported initially in Ref. [77, 78] for LS4 and NS4 glasses, while the CS spectrum is from Ref. [79]. Right panel: Theoretical prediction for the variation of the ^{29}Si isotropic chemical shifts as a function of the mean SiOSi bond angle for the different $Q^{(n)}$ species in (a) $43\text{Na}_2\text{O}-57\text{SiO}_2$ (NS1), $22.5\text{Na}_2\text{O}-77.5\text{SiO}_2$ (NS3), and NS4 and LS4 glasses. The solid lines are linear fits to the data for the different $Q^{(n)}$ species. This panel extracted from Ref. [76] compiles data reported in Ref. [77, 78] for LS4 and NS4 glasses, while the NS1 and NS3 data were reported in Ref. [80].

VI. CONCLUSIONS AND OUTLOOK

In this chapter we have given a brief introduction to the technique of *ab initio* simulations. We have argued that despite the large computational efforts that it requires, this approach is very useful and accurate when a multitude of possible local atomic environments can

coexist, i.e. cases that pose difficulties for effective potentials. Examples are therefore glasses as well as surfaces, thus systems which have a large fraction of structural heterogeneities on the microscopic scale. The goal of this text was not to give an exhaustive overview of the field of *ab initio* simulations since the relevant literature has already become too extensive. Therefore we contented ourself in presenting a few examples that show what current state of the art simulations of this kind can do. As a consequence many interesting and important results on a multitude of systems have not been discussed. Examples are the chalcogenide glasses, i.e. systems that have found a widespread application in systems like infrared lenses, materials for data storage etc... (see Chap. XX by B. Bureau and J. Lucas in the present volume [81]). Since these systems do not contain oxygen, an element that is relatively costly to simulate via *ab initio* simulations, these materials can be simulated with a *relatively* smaller effort per particle and thus the systems sizes and accessible time scales can become quite large [15, 82]. As a consequence, and because of their technological importance, quite a few simulations have been done on these glass-formers and we refer the reader interested in more details to the corresponding literature, see for example Refs. [15, 82–91], as well as the references therein.

A further important topic are glasses that contain or whose surface is exposed to water. Due to the high reactivity of hydrogen, this molecule induces local modification of the structure and hence is able to change the properties of the material even if its concentration is very small. Effective force fields have difficulties to describe this reactivity and hence *ab initio* simulations are *a priori* much more appropriate. However, these latter type of simulations face the difficulty that in reality the concentration of water is small, and hence one needs large systems sizes. As a consequence so far only relatively few simulations have been done on complex glasses that contain water [14, 28, 42, 92–99]. We also mention that many first principles investigations have also been carried out in order to better describe and understand the properties of the charged and neutral defects in amorphous silica, as their presence can strongly affect the performances of electronic and optical devices based on SiO₂ [100–107].

At present the main problem that *ab initio* simulations faces is the large computational effort that it requires. Not only is it expensive to calculate for a given system the forces acting on a given particle, but, as mentioned above, this computational work increases quickly with the number of particles in the system (typically with N^3). Thus if one wants in the future

to access significantly larger system sizes (say $O(10^4)$ atoms in a system with oxygen), one has to avoid this rapid growth of the computational load. This is exactly the goal of some recent new *ab initio* techniques like the so-called “order- N ” algorithms for which the computational cost increase only linearly with the system size [108, 109], the “machine learning” approaches [110], or the second generation of the Car-Parrinello approach [111]. These methods have been introduced in the last few years and are promising approaches to allow accessing in the near future system sizes that are significantly larger than the ones that have been possible to deal with in the past. Despite these advances it will in the near future not be possible to simulate systems with, say, $O(10^5)$ atoms. Systems with such a size or larger, are, however, important to study, e.g., the mechanical behavior of glasses on the meso-scale. Thus such simulations will have to be carried out with effective potentials. But even in this case *ab initio* simulations will be able to play an important role in that they can be used to develop the needed effective potentials. For example one can use the detailed microscopic structure information obtained from an *ab initio* simulations of a given material and feed this information to optimize the parameters present in the effective potentials [112–120]. This approach allows thus to obtain in a systematic manner effective potentials that are reliable regarding the description of the local structure but are computationally inexpensive and hence can be used to access large system sizes or long time scales.

As conclusion we can say that *ab initio* simulations of glasses have become by now a standard technique that allows to measure observables that are of high practical relevance but inaccessible to simulations with effective potentials. Therefore this approach is, despite the fact that it is computationally rather costly, a most useful tool to gain insight into the microscopic properties of glasses and also to develop new type of glasses with exotic compositions.

-
- [1] D. Frenkel and B. Smit, *Understanding molecular simulations: From algorithms to applications* (Academic Press, 1996)
 - [2] M. P. Allen and D. J. Tildesley, *Computer simulations of Liquids* (Oxford University Press, 1986)
 - [3] A. Takada, present volume **xx**, xx (2016)

- [4] J. Kohanoff, *Electronic structure calculations for solids and molecules: Theory and computational methods* (Cambridge University Press, 2006)
- [5] D. Marx and J. Hutter, *Ab initio molecular dynamics: Basic theory and advanced methods* (Cambridge University Press, 2009)
- [6] G. H. Booth, A. Grüneis, G. Kresse, and A. Alavi, *Nature* **493**, 365 (2013)
- [7] J. J. Eriksen, P. Baudin, P. Ettenhuber, K. Kristensen, T. Kjærgaard, and P. Jørgensen, *J. Chem. Theo. and Comp.* **11**, 2984 (2015)
- [8] P. Hohenberg and W. Kohn, *Phys. Rev.* **136**, B864 (1964)
- [9] W. Kohn and L. J. Sham, *Phys. Rev.* **140**, A1133 (1965)
- [10] W. Kohn, *Rev. Mod. Phys.* **71**, 1253 (1999)
- [11] R. O. Jones, *Rev. Mod. Phys.* **87**, 897 (2015)
- [12] K. Burke, *J. Chem. Phys.* **136**, 150901 (2012)
- [13] R. Car and M. Parrinello, *Phys. Rev. Lett.* **55**, 2471 (1985)
- [14] E. Berardo, M. Corno, A. N. Cormack, P. Ugliengo, and A. Tilocca, *RSC Advances* **4**, 36425 (2014)
- [15] J. Akola, P. Jónvári, I. Kaban, I. Voleská, J. Kolář, T. Wágner, and R. O. Jones, *Phys. Rev. B* **89**, 064202 (2014)
- [16] A. Bouzid, S. Le Roux, G. Ori, M. Boero, and C. Massobrio, *J. Chem. Phys.* **143**, 034504 (2015)
- [17] N. Jakse and A. Pasturel, *J. Chem. Phys.* **141**, 094504 (2014)
- [18] L. Pedesseau, S. Ispas, and W. Kob, *Phys. Rev. B* **91**, 134201 (2015)
- [19] L. Pedesseau, S. Ispas, and W. Kob, *Phys. Rev. B* **91**, 134202 (2015)
- [20] D. Plašienka, P. Cifra, and R. Martoňák, *J. Chem. Phys.* **142**, 154502 (2015)
- [21] J. Sarnthein, A. Pasquarello, and R. Car, *Phys. Rev. B* **52**, 12690 (1995)
- [22] J. Sarnthein, A. Pasquarello, and R. Car, *Phys. Rev. Lett.* **74**, 4682 (1995)
- [23] R. Martin, *Electronic Structure: Basic Theory and Practical Methods* (Cambridge University Press, 2004)
- [24] M. Benoit, S. Ispas, P. Jund, and R. Jullien, *Eur. Phys. J. B* **13**, 631 (2000)
- [25] M. Benoit, S. Ispas, and M. E. Tuckerman, *Physical Review B* **64**, 224205 (2001)
- [26] S. Ispas, M. Benoit, P. Jund, and R. Jullien, *Phys. Rev. B* **64**, 214206 (2001)
- [27] D. Donadio, M. Bernasconi, and F. Tassone, *Phys. Rev. B* **70**, 214205 (2004)

- [28] M. Pöhlmann, M. Benoit, and W. Kob, *Phys. Rev. B* **70**, 184209 (2004)
- [29] J. Du and L. R. Corrales, *J. Chem. Phys.* **125**, 114702 (2006)
- [30] R. Vuilleumier, N. Sator, and B. Guillot, *Geochim. et Cosmochim. Acta* **73**, 6313 (2009)
- [31] N. Jakse, M. Bouhadja, J. Kozaily, J. W. E. Drewitt, L. Hennet, D. R. Neuville, H. E. Fischer, V. Cristiglio, and A. Pasturel, *Appl. Phys. Lett.* **101**, 201903 (2012)
- [32] G. Spiekermann, M. Steele-MacInnis, P. M. Kowalski, C. Schmidt, and S. Jahn, *Chem. Geology* **346**, 22 (2013)
- [33] R. Vuilleumier, A. P. Seitsonen, N. Sator, and B. Guillot, *Chem. Geology* **418**, 77 (2015)
- [34] L. Giacomazzi, P. Umari, and A. Pasquarello, *Phys. Rev. Lett.* **95**, 075505 (2005)
- [35] S. Ohmura and F. Shimojo, *Phys. Rev. B* **78**, 224206 (2008)
- [36] G. Ferlat, T. Charpentier, A. P. Seitsonen, A. Takada, M. Lazzeri, L. Cormier, G. Calas, and F. Mauri, *Phys. Rev. Lett.* **101**, 065504 (2008)
- [37] S. Ohmura and F. Shimojo, *Phys. Rev. B* **80**, 020202 (2009)
- [38] J. P. Hansen and I. R. McDonald, *Theory of Simple Liquids* (Academic, London, 1986)
- [39] K. Binder and W. Kob, *Glassy Materials and disordered solids* (World Scientific, 2011)
- [40] S. W. Lovesey, *Theory of neutron scattering from condensed matter* (Clarendon Press, Oxford, 1984)
- [41] D. Waasmaier and A. Kirfel, *Acta Crystallographica* **A51**, 416 (1995)
- [42] A. Tilocca and A. N. Cormack, in *Proceedings of the Royal Society of London A: Mathematical, Physical and Engineering Sciences*, Vol. 467 (The Royal Society, 2011) pp. 2102–2111
- [43] J. Sarnthein, A. Pasquarello, and R. Car, *Science* **275**, 1925 (1997)
- [44] A. Pasquarello, J. Sarnthein, and R. Car, *Phys. Rev. B* **57**, 14133 (1998)
- [45] M. Benoit and W. Kob, *EPL (Europhysics Letters)* **60**, 269 (2002)
- [46] L. Giacomazzi, P. Umari, and A. Pasquarello, *Phys. Rev. B* **79**, 064202 (2009)
- [47] R. Haworth, G. Mountjoy, M. Corno, P. Ugliengo, and R. J. Newport, *Phys. Rev. B* **81**, 060301 (2010)
- [48] S. Ispas, N. Zotov, S. De Wispelaere, and W. Kob, *J. Non-Cryst. Solids* **351**, 1144 (2005)
- [49] P. Ganster, M. Benoit, J.-M. Delaye, and W. Kob, *Mol. Sim.* **33**, 1093 (2007)
- [50] M. Corno, A. Pedone, R. Dovesi, and P. Ugliengo, *Chem. Mat.* **20**, 5610 (2008)
- [51] M. T. Dove, *Introduction to lattice dynamics* (Cambridge University Press, 1993)
- [52] S. Taraskin and S. Elliott, *Phys. Rev. B* **55**, 117 (1997)

- [53] L. Huang and J. Kieffer, in *Molecular Dynamics Simulations of Disordered Materials* (Springer, 2015) pp. 87–112
- [54] B. Van Beest, G. J. Kramer, and R. Van Santen, *Phys. Rev. Lett.* **64**, 1955 (1990)
- [55] K. Vollmayr, W. Kob, and K. Binder, *Phys. Rev. B* **54**, 15808 (1996)
- [56] J. Carpenter and D. Price, *Phys. Rev. Lett.* **54**, 441 (1985)
- [57] E. Fabiani, A. Fontana, and U. Buchenau, *J. Chem. Phys.* **128**, 244507 (2008)
- [58] G. Henderson, present volume **xx**, xx (2016)
- [59] X. Gonze and C. Lee, *Phys. Rev. B* **55**, 10355 (1997)
- [60] A. Pasquarello and R. Car, *Phys. Rev. Lett.* **79**, 1766 (1997)
- [61] M. F. Thorpe and S. W. de Leeuw, *Phys. Rev. B* **33**, 8490 (1986)
- [62] E. I. Kamitsos, J. A. Kapoutsis, H. Jain, and C. H. Hsieh, *J. Non-Cryst. Solids* **171**, 31 (1994)
- [63] H. Philipp, “Silicon dioxide (SiO₂) (glass),” in *Handbook of Optical Constants of Solids* (ed. D. Palik, Academic Press, San Diego, 1998) pp. 749–763
- [64] D. D. S. Meneses, M. Eckes, L. Del Campo, C. N. Santos, Y. Vaills, and P. Echegut, *Vibr. Spectro.* **65**, 50 (2013)
- [65] F. Domine and B. Piriou, *J. Non-Cryst. Solids* **55**, 125 (1983)
- [66] C. I. Merzbacher and W. B. White, *Amer. Miner.* **73**, 1089 (1988)
- [67] P. Umari, A. Pasquarello, and A. Dal Corso, *Phys. Rev. B* **63**, 094305 (2001)
- [68] M. Lazzeri and F. Mauri, *Phys. Rev. Lett.* **90**, 036401 (2003)
- [69] P. Umari, X. Gonze, and A. Pasquarello, *Phys. Rev. Lett.* **90**, 027401 (2003)
- [70] P. Umari and A. Pasquarello, *Phys. Rev. Lett.* **95**, 137401 (2005)
- [71] P. Umari and A. Pasquarello, *Phys. Rev. Lett.* **98**, 176402 (2007)
- [72] J. F. Stebbins, present volume **xx**, xx (2016)
- [73] C. J. Pickard and F. Mauri, *Phys. Rev. B* **63**, 245101 (2001)
- [74] D. Sebastiani and M. Parrinello, *J. Phys. Chem. A* **105**, 1951 (2001)
- [75] T. Charpentier, *Solid state nuclear magnetic resonance* **40**, 1 (2011)
- [76] T. Charpentier, M. C. Menziani, and A. Pedone, *RSC Advances* **3**, 10550 (2013)
- [77] T. Charpentier, S. Ispas, M. Profeta, F. Mauri, and C. J. Pickard, *J. Phys. Chem. B* **108**, 4147 (2004)
- [78] S. Ispas, T. Charpentier, F. Mauri, and D. R. Neuville, *Sol. St. Sciences* **12**, 183 (2010)

- [79] A. Pedone, T. Charpentier, and M. C. Menziani, *Phys. Chem. Chem. Phys.* **12**, 6054 (2010)
- [80] F. Angeli, O. Villain, S. Schuller, S. Ispas, and T. Charpentier, *Geochim. et Cosmochim. Acta* **75**, 2453 (2011)
- [81] B. Bureau and J. Lucas, present volume **xx**, xx (2016)
- [82] A. Bouzid, S. Gabardi, C. Massobrio, M. Boero, and M. Bernasconi, *Phys. Rev. B* **91**, 184201 (2015)
- [83] S. Blaineau and P. Jund, *Phys. Rev. B* **70**, 184210 (2004)
- [84] L. Giacomazzi, C. Massobrio, and A. Pasquarello, *Phys. Rev. B* **75**, 174207 (2007)
- [85] I. Chaudhuri, F. Inam, and D. Drabold, *Phys. Rev. B* **79**, 100201 (2009)
- [86] C. Massobrio, M. Celino, P. S. Salmon, R. A. Martin, M. Micoulaut, and A. Pasquarello, *Phys. Rev. B* **79**, 174201 (2009)
- [87] T. Lee, S. Simdyankin, J. Hegedus, J. Heo, and S. R. Elliott, *Phys. Rev. B* **81**, 104204 (2010)
- [88] S. Le Roux, A. Bouzid, M. Boero, and C. Massobrio, *J. Chem. Phys.* **138**, 174505 (2013)
- [89] M. Bauchy, A. Kachmar, and M. Micoulaut, *J. Chem. Phys.* **141**, 194506 (2014)
- [90] M. Micoulaut, M.-V. Coulet, A. Piarristeguy, M. Johnson, G. Cuello, C. Bichara, J.-Y. Raty, H. Flores-Ruiz, and A. Pradel, *Phys. Rev. B* **89**, 174205 (2014)
- [91] J. Y. Raty, W. Zhang, J. Luckas, C. Chen, R. Mazzarello, C. Bichara, and M. Wuttig, *Nature Comm.* **6** (2015)
- [92] C. Mischler, W. Kob, and K. Binder, *Comp. Phys. Comm.* **147**, 222 (2002)
- [93] F. Bouyer, G. Geneste, S. Ispas, W. Kob, and P. Ganster, *J. Solid State Chem.* **183**, 2786 (2010)
- [94] A. Tilocca and A. N. Cormack, *ACS Appl. Mat. & Interf.* **1**, 1324 (2009)
- [95] A. Tilocca, *J. Mat. Chem.* **20**, 6848 (2010)
- [96] A. A. Hassanali, H. Zhang, C. Knight, Y. K. Shin, and S. J. Singer, *J. Chem. Theo. Comp.* **6**, 3456 (2010)
- [97] G. Spiekermann, M. Steele-MacInnis, C. Schmidt, and S. Jahn, *J. Chem. Phys.* **136**, 154501 (2012)
- [98] Á. Cimas, F. Tielens, M. Sulpizi, M.-P. Gaigeot, and D. Costa, *J. Phys.: Condens. Matter* **26**, 244106 (2014)
- [99] G. Spiekermann, M. Wilke, and S. Jahn, *Chem. Geology*(2016)
- [100] M. Boero, A. Pasquarello, J. Sarnthein, and R. Car, *Phys. Rev. Lett.* **78**, 887 (1997)

- [101] T. Bakos, S. Rashkeev, and S. Pantelides, *Phys. Rev. B* **70**, 075203 (2004)
- [102] L. Martin-Samos, Y. Limoge, N. Richard, J. Crocombette, G. Roma, E. Anglada, and E. Artacho, *EPL (Europhysics Letters)* **66**, 680 (2004)
- [103] L. Martin-Samos, Y. Limoge, J.-P. Crocombette, G. Roma, N. Richard, E. Anglada, and E. Artacho, *Phys. Rev. B* **71**, 014116 (2005)
- [104] T. Uchino and T. Yoko, *Phys. Rev. B* **74**, 125203 (2006)
- [105] J. Du, L. R. Corrales, K. Tsemekhman, and E. J. Bylaska, *Nuclear Instruments and Methods in Physics Research Section B: Beam Interactions with Materials and Atoms* **255**, 188 (2007)
- [106] N. L. Anderson, R. P. Vedula, P. A. Schultz, R. M. Van Ginhoven, and A. Strachan, *Phys. Rev. Lett.* **106**, 206402 (2011)
- [107] L. Giacomazzi, L. Martin-Samos, A. Boukenter, Y. Ouerdane, S. Girard, and N. Richard, *Phys. Rev. B* **90**, 014108 (2014)
- [108] D. Bowler, R. Choudhury, M. Gillan, and T. Miyazaki, *Phys. Stat. Sol. (b)* **243**, 989 (2006)
- [109] N. D. Hine, P. D. Haynes, A. A. Mostofi, C.-K. Skylaris, and M. C. Payne, *Comp. Phys. Comm.* **180**, 1041 (2009)
- [110] M. Caccin, Z. Li, J. R. Kermode, and A. De Vita, *Inter. J. Quant. Chem.* **115**, 1129 (2015), <http://dx.doi.org/10.1002/qua.24952>
- [111] T. D. Kuhne, *Wiley Interdiscip. Rev.: Comput. Mol. Sci.* **4**, 391 (2014)
- [112] P. Tangney and S. Scandolo, *J. Chem. Phys.* **117**, 8898 (2002)
- [113] S. Jahn and P. A. Madden, *Phys. Earth and Planetary Int.* **162**, 129 (2007)
- [114] A. Carré, J. Horbach, S. Ispas, and W. Kob, *EPL (Europhysics Letters)* **82**, 17001 (2008)
- [115] A. Pedone, G. Malavasi, M. C. Menziani, U. Segre, F. Musso, M. Corno, B. Civalleri, and P. Ugliengo, *Chem. Mat.* **20**, 2522 (2008)
- [116] J. R. Kermode, S. Cereda, P. Tangney, and A. De Vita, *J. Chem. Phys.* **133**, 094102 (2010)
- [117] D. Marrocchelli, M. Salanne, P. A. Madden, C. Simon, and P. Turq, *Mol. Phys.* **107**, 443 (2009)
- [118] S. Izvekov and B. M. Rice, *J. Chem. Phys.* **136**, 134508 (2012)
- [119] A. Zeidler, K. Wezka, D. A. Whittaker, P. S. Salmon, A. Baroni, S. Klotz, H. E. Fischer, M. C. Wilding, C. L. Bull, and M. G. Tucker, *Phys. Rev. B* **90**, 024206 (2014)
- [120] S. Izvekov and B. M. Rice, *J. Chem. Phys.* **143**, 244506 (2015)